Micromagnetics and multiscale hysteresis simulations of permanent magnets

Yangyiwei Yang, Patrick Kühn, Mozhdeh Fathidoost and Bai-Xiang Xu
Mechanics of Functional Materials Division, Technische Universität Darmstadt, Darmstadt, Germany

Received 18 December 2022
Revised 2 August 2023
Accepted 18 August 2023

Abstract

Purpose – Confronting the unveiled sophisticated structural and physical characteristics of permanent magnets, notably the samarium–cobalt (Sm-Co) alloy, This work aims to introduce a simulation scheme that can link physics-based micromagnetics on the nanostructures and magnetostatic homogenization on the mesoscale polycrystalline structures.

Design/methodology/approach – The simulation scheme is arranged in a multiscale fashion. The magnetization behaviors on the nanostructures examined with various orientations are surrogated as the micromagnetic-informed hysterons. The hysteresis behavior of the mesoscale polycrystalline structures with micromagnetic-informed hysterons is then evaluated by computational magnetostatic homogenization.

Findings – The micromagnetic-informed hysterons can emulate the magnetization reversal of the parameterized Sm-Co nanostructures as the local hysteresis behavior on the mesostructures. The simulation results of the mesoscale polycrystal demonstrate that the demagnetization process starts from the grain with the largest orientation angle (a) and then propagates to the surrounding grains.

Research limitations/implications – The presented scheme depicts the demand for integrating data-driven methods, as the parameters of the surrogate hysteron intrinsically depend on the nanostructure and its orientation. Further hysteron parameters that help the surrogate hysteron emulate the micromagnetic-simulated magnetization reversal should be examined.

Originality/value – This work provides a novel multiscale scheme for simulating the polycrystalline permanent magnets' hysteresis while recapitulating the nanoscale mechanisms, such as the nucleation of domains, and domain wall migration and pinning. This scheme can be further extended to simulate the part-level hysteresis considering the mesoscale features.

Keywords Micromagnetics, Magnetostatic homogenization, Permanent magnets, Polycrystal

Paper type Research paper

The authors acknowledge the financial support of German Science Foundation (DFG) in the framework of the Collaborative Research Centre Transregio 270 (CRC-TRR 270, project number 405553726, subprojects A06, B13) and 361 (CRC-TRR 361, project number 492661287, subprojects A05). The authors also greatly appreciate their access to the Lichtenberg High-Performance Computer and the technical supports from the HHLR, Technische Universität Darmstadt and the GPU Cluster from the CRC-TRR 270 subproject Z-INF.

COMPEL - The international journal for computation and mathematics in electrical and electronic engineering
Vol. 42 No. 5, 2023
pp. 993-1006
Emerald Publishing Limited
0332-1649
DOI 10.1108/COMPEL-12-2022-0424

1. Motivations

Due to its superior corrosion resistance under complex chemical environment and outstanding stability at high temperature, samarium–cobalt (Sm-Co)-based magnets have promised industries feasibility in various applications, such as high-performance electric motors for automotive and aeronautic application. However, former researches have unveiled the microstructure of such permanent magnets in a sophisticated multiscale fashion. As shown in Figure 1, it has been investigated that commercial Sm-Co magnets present a three-phase composite nanostructure (<1 μm). This nanostructure can be described as the cellular Sm_2Co_{17} phase surrounded by a coherent stripe-shaped $SmCo_5$ phase. This is further subdivided by the Zr-rich platelet-shaped phases (hereinafter referred to as Z-platelets) which develop perpendicular to the crystallographic *c*-axis of the Sm_2Co_{17} phase (Duerrschnabel *et al.*, 2017; Katter *et al.*, 1996; Song *et al.*, 2020; Gutfleisch, 2009). The final nanostructure depends on the chemical composition and thermal treatments (Wang and Zhu, 2021). Notably, Zhou *et al.* (2021) reported increases in thickness of Z-platelets from 2.4 nm up to 28.8 nm with only an increase in annealing time. Meanwhile, as one of the commercial permanent magnets that is manufactured by sintering, polycrystalline structure on the mesoscale (1–100 μm) is also observed and examined in Sm-Co alloy (Giron *et al.*, 2022).

Most of the primary mechanisms contributing to the magnetic behavior (i.e. nucleation of the reversed domain, and migration/pinning of the domain wall) occur on the nanoscale with characteristic length around 1 nm, while receiving effects from grain orientation and local thermal history, hysteresis behavior varies locally on the level of the polycrystal. This stresses the importance of scale-bridging on accurate modeling and simulation of the hysteresis behavior. Although there are well-established models for individual scales, scale-bridging strategy is intricate and essential. It is worth noting that the strategy bridging the atomic and nanoscale micromagnetic combining first-principles calculations, atomistic spin model simulations and micromagnetic simulations has been investigated and discussed (Gong, 2022). Nevertheless, the strategy bridging the nanoscale and mesoscale is still

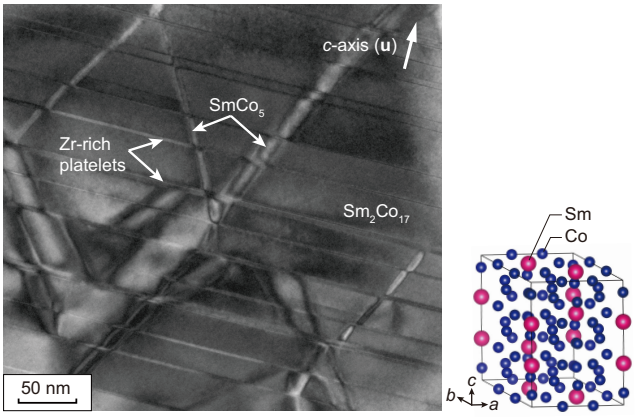

Figure 1.
Bright-field TEM image of the Sm-Co magnets containing nanoscopic $SmCo_5$, Sm_2Co_{17} and Zr-rich phases

Note: The lattice structure as well as the crystallographic axes of Sm_2Co_{17} are presented as the inset
Source: Figure courtesy of Duerrschnabel *et al.* (2017) under the terms of the Creative Commons CC-BY license

missing. On the other hand, macroscopic hysteresis behavior can be directly modeled using proposed phenomenological models, such as the Preisach's (Preisach, 1935), Takács's (Takács, 2001) and Jiles-Atherton's model (Jiles and Atherton, 1984; Zirka *et al.*, 2012). These models, however, fail to deliver the physics information on individual scales and cannot be used in the sense of tailoring hysteresis of permanent magnets.

At the end of the day, modeling and simulating the hysteresis of the permanent magnets demands a multiscale scenario bridging mesoscale phenomena and nanoscale mechanisms, which becomes the objective of this work. We propose a novel multiscale scheme for simulating the polycrystalline permanent magnets' hysteresis combining the merits of both micromagnetics and computational magnetostatic homogenization. This scheme is also extendable to simulate the part-level hysteresis and is capable of integrating machine-learning-based data-driven methods. It is hoped that the present work can serve a new viewpoint/methodology in the field of electromagnetic engineering in the hysteresis behavior of magnetic materials and components and provide a computational toolkit that is practicable and physics-rooted.

2. Models and methods

Figure 2 presents the workflow of proposed multiscale hysteresis simulation for the polycrystalline permanent magnets. We start with performing a series of micromagnetic simulations on distinct parameterized nanostructures. Micromagnetics has a sound physics foundation and thus is suitable for investigating local magnetization switching mechanisms. To have acceptable computational cost-efficiency with fine spatial discretization for resolving physical processes (e.g. domain nucleation, and domain wall migration and pinning), micromagnetic simulations are implemented and performed by the finite difference method (FDM). Next, the surrogate hysteresis unit (or "hysteron," adopted from its pseudo-particle behavior) parameterized by the results of micromagnetics is used to replace micromagnetic calculations on the mesoscale polycrystalline structures. This hysteron should preserve the physical characteristics unveiled by the micromagnetics, such as the local magnetic coercivity and magnetization rotation. Finally, the hysteresis behavior of the polycrystalline structure with micromagnetics-informed hysterons is evaluated by computational magnetostatic homogenization. Due to the need for geometrically

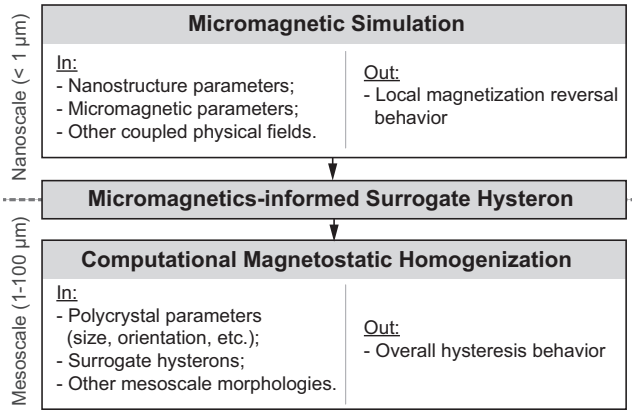

Source: Authors' own work

Figure 2. Workflow of the proposed multiscale hysteresis simulation scheme

complicated polycrystalline structures without compromising in numerical accuracy, magnetostatic homogenizations are implemented and performed by the finite element method (FEM).

It is worth noting that the magnetization reversal on each level of the proposed scheme is modeled and simulated under the equilibrium conditions, which is sufficient for evaluating the material- and structural-based hysteresis behavior without loss. It also helps reduce the 3D magnetization dynamics (a.k.a. Landau–Lifshitz–Gilbert dynamics) to 2D rotational one (a.k.a. Stoner–Wohlfarth reversal, where magnetization is also in the plane defined by the magnetic field **H** and the easy axis **u**).

2.1 Micromagnetics

Below the Curie temperature, the magnetization of most of magnetic materials saturates with constant magnitude (M_{sat}). Therefore, in the micromagnetics, it is important to have the normalized magnetization vector which is position dependent, i.e. **m**(**r**). This vector field can be physically interpreted as the mean field of the local atomic magnetic moments, but yet sufficiently small in scale to resolve the magnetization transition across the domain wall. In this regard, we consider the free energy density functional of a micromagnetic system (with a volume V) as the functional of **m**(**r**), i.e.:

$$\mathcal{F} = \int_V \left[f_{\text{ex}} + f_{\text{ani}} + f_{\text{ms}} + f_{\text{zm}} + f_{\text{cp}} \right] \mathrm{d}V. \tag{1}$$

where f_{ex} is the exchange contribution, recapitulating the parallel-aligning tendency among neighboring magnetic moments due to the Heisenberg exchange interaction. In that sense, this term acts as a thermodynamic penalty to the system at the domain wall and provides the local driving force to the domain wall migration. By defining a positive exchange parameter A_{ex}, this term is formulated as:

$$f_{\text{ex}} = A_{\text{ex}} ||\nabla \mathbf{m}||^2. \tag{2}$$

The term f_{ani} represents the contribution due to the magnetocrystalline anisotropy. It provides the energetically preferred orientation to local magnetizations, which is related to the defined easy axis **u** mostly of the material. Sm-Co permanent magnets generally possess crystalline structures with uniaxial anisotropy with **u** parallel to the crystallographic c-axis, which is perpendicular to the Zr-rich platelet phase, as shown in Figure 1 (Gutfleisch, 2009). In this regard, f_{ani} is formulated as:

$$f_{\text{ani}} = -\sum_i K_{ui} (\mathbf{u} \cdot \mathbf{m})^{2i}. \tag{3}$$

It is worth noting that most of the investigations only use the lowest order ($i = 1$) with the characteristic parameter K_{u1}. It can be shown that the parameters A_{ex} and K_{u1} are related to the Bloch domain wall energy σ_{dw} and width l_{dw} of the materials at the equilibrium as:

$$\sigma_{\text{dw}} = 4\sqrt{A_{\text{ex}} K_{\text{u1}}} \quad \text{and} \quad l_{\text{dw}} = \pi \sqrt{\frac{A_{\text{ex}}}{K_{\text{u1}}}} \tag{4}$$

where SI units are used (Kronmüller, 2003). Normally, A_{ex}, K_{u1} and M_{sat} are obtained from either experimental measurements or from ab initial calculation.

Besides f_{ex} and f_{ani} which are material-dependent, the terms f_{ms}, f_{zm} and f_{cp} provide the contributions due to the interaction among magnetization and distinct intrinsic/extrinsic fields and thereby change the local thermodynamic stability. The magnetostatic term f_{ms} takes account of the energy of each local magnetization (or a magnetic moment) under the demagnetizing field created by the surrounding magnetization (or by all the other magnetic moments). It is generally formulated as:

$$f_{ms} = -\frac{1}{2}\mu_0 M_{sat}\mathbf{m}\cdot\mathbf{H}_{dm}, \tag{5}$$

where the calculation of the demagnetizing field $\mathbf{H}_{dm}$ highly depends on the choice of the boundary condition (BC), and M_{sat} is the saturated magnetization of the material. Similarly, the Zeeman and multiphysics-coupling terms f_{zm} and f_{cp}, correspondingly taking account of the energy of each local magnetization under an extrinsic magnetic field $\mathbf{H}$ and an effective field induced by the coupled physical effects $\mathbf{H}_{cp}$, are formulated as:

$$f_{zm} = -\mu_0 M_{sat}\mathbf{m}\cdot\mathbf{H}, \tag{6}$$

$$f_{cp} = -\mu_0 M_{sat}\mathbf{m}\cdot\mathbf{H}_{cp}. \tag{7}$$

The exact formulation of the coupling field $\mathbf{H}_{cp}$ depends on the choice of coupled physical effects, such as magnetostriction (Kronmüller, 2003), thermal fluctuation (Brown, 1963) and spin-current interactions (Sun, 2000).

Generally, $\mathbf{H}$ is implemented as a controllable quantity for the investigator to emulate the magnetic loading/unloading as in the experiments, i.e. an applied magnetic field $\mathbf{H}_{ext}$, and the micromagnetic system should find its equilibrium. This is mathematically determined as follows:

$$\underbrace{\mathbf{m}\times\frac{\delta\mathcal{F}}{\delta\mathbf{m}}}_{-\boldsymbol{\tau}_{prec}} + \underbrace{\alpha_d\mathbf{m}\times\left(\mathbf{m}\times\frac{\delta\mathcal{F}}{\delta\mathbf{m}}\right)}_{-\boldsymbol{\tau}_{damp}} = 0$$
$$\text{subject to} \quad ||\mathbf{m}|| = 1. \tag{8}$$

Equation (8) can be physically interpreted as the balance between two components of Landau–Lifshitz torque that, respectively, contribute to the precession ($\boldsymbol{\tau}_{prec}$) and the damping ($\boldsymbol{\tau}_{damp}$) actions of the magnetization $\mathbf{m}$ (Gilbert, 1955; Coey, 2010), where α_d is the damping coefficient. As the precession direction of the $\mathbf{m}$ is always perpendicular to both $\mathbf{m}$ and the effective field $\mathbf{H}_{eff} \equiv -\delta\mathcal{F}/\delta\mathbf{m}$, the term $\boldsymbol{\tau}_{prec}$ presents thereby no contribution to the magnetization reversal process, when $\mathbf{m}$ evolves from antiparallel to parallel with respect to (w.r.t.) $\mathbf{H}_{eff}$. In that sense, only the damping term of equation (8) remains for solving thermodynamically preferred $\mathbf{m}(\mathbf{r})$ under an applied $\mathbf{H}_{ext}$, i.e.:

$$\mathbf{m}\times\left(\mathbf{m}\times\frac{\delta\mathcal{F}}{\delta\mathbf{m}}\right) = 0 \quad \text{subject to} \quad ||\mathbf{m}|| = 1. \tag{9}$$

In this work, the FDM-based steepest conjugate gradient (SCG) method is used for solving equation (9) by the merit of its speed, cost-efficiency and capability for GPU-parallel

implementation (Leliaert *et al.*, 2018). Another key advantage of using FDM-based SCG method is to obtain the demagnetizing field $\mathbf{H}_{\mathrm{dm}}$ directly by magnetostatic convolution of $\mathbf{m}$ over the simulation domain without introducing additional degrees of freedom (Vansteenkiste *et al.*, 2014; McMichael *et al.*, 1999). In this regard, BCs of $\mathbf{m}$ become significant for correct evaluation of $\mathbf{H}_{\mathrm{dm}}$. Two BCs are majorly used in simulating the magnetization reversal inside magnetic materials: the Neumann BC ($\nabla\mathbf{m}|_{\partial V}\cdot\mathbf{n}=0$ with $\mathbf{n}$ the normal vector of the boundary ∂V) represents that the neighboring magnetizations outside of the simulation domain are identical to the ones at the boundary (Donahue and Porter, 2004); the Periodic BC represents that the spatial distribution of the magnetizations inside the simulation domain repeats itself periodically along prescribed directions (Fangohr *et al.*, 2009).

Based on SCG method, the iteration scheme for calculating the magnetization is formulated as follows with a descending direction $\mathbb{H}_n$, i.e.:

$$\begin{aligned}\mathbf{m}_{n+1} &= \mathbf{m}_n - \delta_n \mathbb{H}_n,\\ \mathbb{H}_n &= \mathbf{m}_n^* \times \nabla_{\mathbf{m}} \hat{\mathcal{F}}(\mathbf{m}_n, \mathbf{H}) \times \mathbf{m}_n.\end{aligned} \tag{10}$$

Here, $\mathbf{m}_n^* = \mathbf{m}^n$ will derive $\mathbb{H}_n$ as the steepest searching direction, and $\mathbf{m}_n^* = (\mathbf{m}_n + \mathbf{m}_{n+1})/2$ as the curvilinear searching direction on the sphere (Goldfarb *et al.*, 2009). $\hat{\mathcal{F}}(\mathbf{m}_n, \mathbf{H})$ is the free energy on the discretized domain. The step length δ_n is initialized by an inexact line search and subsequentially obtained by the Barzilai–Borwein rule. This method has been implemented by FDM in the package MuMax^3 (Vansteenkiste *et al.*, 2014) with details elaborated in (Exl *et al.*, 2014).

2.2 Micromagnetics-informed surrogate hysteron

To correctly simulate the local magnetization reversal and associated domain wall migration, sufficiently fine space discretization (mesh) is required to resolve the reversed nucleus formed near grain edges/corners where the demagnetizing field is high (Yi *et al.*, 2016), and the transition profile of magnetization across the domain wall with its thickness characterized by l_{dw}. As most permanent magnets with l_{dw} in the range of several nanometers, e.g. $l_{\mathrm{dw}} \sim 2$ nm for Nd-Fe-B and Sm-Co magnets and $l_{\mathrm{dw}} \sim 50$ nm for electrical steels (4.6% Si), it is impractical in both numerical and computational senses for direct micromagnetic calculations on the mesoscale structure of such materials, where the spatial distribution of grains with distinct sizes and orientations (easy axes) is believed to have significant influences as well. In this regard, a surrogate model is required to equivalently replace the direct micromagnetic calculation on every subdomain for the hysteresis simulation on the polycrystal level. Such a surrogate model:

- can efficiently describe the local magnetization reversal as an isolated unit but also as the representative component (subsystem) of the polycrystal system. Such local reversal should be also dependent on the given orientation of the subdomain; and
- can preserve the important characteristics of the local magnetization reversal by the micromagnetics, e.g. the local magnetic coercivity H_c where the magnetization of the chosen subsystem cannot withstand the applied field and gets reversed.

In this work, we use the vector hysteron as the surrogate model of the micromagnetic simulations, which can well describe the magnetization reversal of the ferromagnetic domain at equilibrium. Each vector hysteron can be regarded as an independent Stoner–Wohlfarth pseudo-particle, as its magnetization can only rotate freely in the plane defined

by the magnetic field **H** and the easy axis **u** (if **H**||**u**, then the hard axis perpendicular to **u** should be provided instead), as shown schematically in the inset of Figure 3. A hysteron inside a system (as an assembly of hysterons) can only affect the neighboring one via magnetostatic interactions, in other words, by affecting the local magnetic field.

This vector hysteron consists of two major parameters: the local switching field H_{sw} and the orientation angle α. Defining the local coordinates by the defined positive direction of the applied magnetic field, i.e. $\mathbf{H} = H\mathbf{h}_{\parallel}$, the longitudinal magnetization of a single demagnetizing process (simplified as H reversely increasing) is analytically formulated as:

$$\mathbf{m}(H) = \begin{cases} m^{\parallel}_{[-]}\mathbf{h}_{\parallel} + m^{\perp}_{[-]}\mathbf{h}_{\perp} & H < -H_{sw} \\ m^{\parallel}_{[+]}\mathbf{h}_{\parallel} + m^{\perp}_{[+]}\mathbf{h}_{\perp} & \text{otherwise} \end{cases} \tag{11}$$

with:

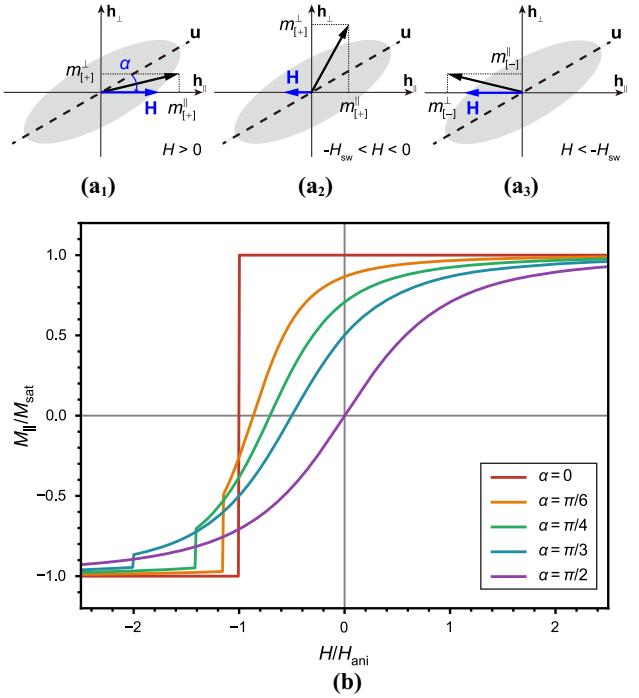

Notes: (a_1) $H > 0$; (a_2) $-H_{sw} < H < 0$; (a_3) $H < -H_{sw}$. $m^{\parallel}_{[\pm]}$ and $m^{\perp}_{[\pm]}$ and are, respectively, the longitudinal and transverse magnetization components with [+] for the upper branch and [−] for the lower branch. $\mathrm{H} = H\mathbf{h}_{\parallel}$; (b) Longitudinal half-cycle hysteresis of parameterized vector hysteron with different easy axis orientations

Source: Authors' own work

Figure 3. Pseudo-particles schematic of the vector hysteron with easy axis **u**, which presents the equilibrium magnetization at the varying field

$$m_{[\pm]}^{||} = \frac{H \pm H_{sw}\cos\alpha}{\sqrt{H^2 \pm 2HH_{sw}\cos\alpha + H_{sw}^2}}, \tag{12}$$

where the plus sign for the upper branch and the minus sign for the lower branch (Petrila and Stancu, 2011). The transverse magnetization $m_{[\pm]}^{\perp} = \sqrt{1 - \left(m_{[\pm]}^{||}\right)^2}$ is calculated accordingly. The reversal of magnetization vector represented by equation (11) with prescribed α is schematically presented in Figure 3(a). The switching field H_{sw} should be intrinsically structure- and orientation-dependent and should be examined on varying nanostructures. We take the following H_{sw} to separate the dependence from a set of nanostructure parameters $\{s\}$ and the orientation α:

$$H_{sw}(\alpha, \{s\}) = \frac{H_{ani}(\{s\})}{\cos\alpha} + H_l(\alpha, \{s\}). \tag{13}$$

where $H_{ani}(\{s\})$ is physically regarded as the anisotropic field of a nanostructure. For homogeneous ferromagnetic materials, $H_{ani} = 2K_1/\mu_0 M_{sat}$. The longitudinal shifting field $H_l(\alpha, \{s\})$ is to recapitulate the associate effects that might influence the magnetization reversal (like the pinning effects). Taking $H_l = 0$, the half-cycle hysteresis curves presented by equation (11) with varying α are illustrated in Figure 3(b), where we can observe the cut-off switching of the magnetization once reaching H_{sw} (Petrila and Stancu, 2011). In this work, $H_{sw}(\alpha)$ is the major parameter that is informed by micromagnetic simulations. It is expected to optimize the formulation of H_{sw} and further investigate its structural dependence adopting the data-driven scenario in our works in the near future.

2.3 Computational magnetostatic homogenization

In this work, the overall hysteresis behavior of the polycrystal is examined by performing computational magnetostatic homogenization. The governing equations for magnetostatics are derived by eliminating the time derivative terms in Maxwell's equations as:

$$\nabla \times \mathbf{H} = \mathbf{J}, \tag{14}$$

$$\nabla \cdot \mathbf{B} = 0, \tag{15}$$

where $\mathbf{B}$ is the magnetic flux density, and $\mathbf{J}$ is the current density. In this work, we consider the case when no current density appears in the system ($\mathbf{J} = \mathbf{0}$), which means $\mathbf{H}$ is a curl-free vector field, i.e. $\nabla \times \mathbf{H} = \mathbf{0}$. In that sense, we can calculate the magnetic field by using merely the magnetic scalar potential Φ, i.e. $\mathbf{H} = -\nabla\Phi$. Considering the constitutive relation of magnetostatic, i.e. $\mathbf{B} = \mu_0[\mathbf{H} + \mathbf{M}(\mathbf{H})]$ with $\mathbf{M}(\mathbf{H})$ the local magnetization, the Gaussian law in equation (15) is then rewritten in the Laplace form to be the governing equation of the system:

$$\Delta\Phi - \nabla \cdot \mathbf{M} = 0. \tag{16}$$

Omitting Ampère's law in equation (14) by assuming no space current density also disregards the effects of eddy current. The homogenization scheme considering the eddy current losses is in development and will be discussed in upcoming works.

The magnetostatic homogenization problem can then be defined as:

$$\begin{cases} \mathbf{B} = \mu_0[\mathbf{H} + \mathbf{M}(\mathbf{H})] & \text{on microscale,} \\ \langle \mathbf{B} \rangle = \mu_0[\langle \mathbf{H} \rangle + \langle \mathbf{M} \rangle] & \text{on macroscale,} \end{cases} \tag{17}$$

where $\langle \cdot \rangle = \int_V (\cdot) \mathrm{d}V/V$, and V here is the volume of the simulation domain. By using the micromagnetics-informed surrogate hysteron, the local magnetization **M(H)** not only readily recapitulates the magnetization reversal determined by the nanostructure and micromagnetic contributions but also reflects the orientation-dependences on the polycrystal level. $\langle \mathbf{H} \rangle$ is provided by linear BC of scalar potential that satisfies the Hill–Mandel condition $\langle \mathbf{B} \cdot \mathbf{H} \rangle = \langle \mathbf{B} \rangle \cdot \langle \mathbf{H} \rangle$, i.e.:

$$\Phi|_{\partial V} = -\mathbf{H}_{\text{ext}} \cdot \mathbf{r}|_{\partial V}, \tag{18}$$

where $\mathbf{H}_{\text{ext}}$ is constantly prescribed, and $\mathbf{r}$ represents the coordinates. Equations (16)–(18) are implemented by FEM in the package NIsoS developed by authors based on MOOSE framework (Tonks *et al.*, 2012; Permann *et al.*, 2020). Four-node tetrahedron Lagrangian elements are chosen to mesh the geometry. A transient solver with preconditioned Jacobian-Free Newton–Krylov method and backward Euler algorithm is used. Randomly seeded polycrystalline structures as well as corresponding meshes are created using the open-source package Neper (Quey *et al.*, 2011; Quey and Renversade, 2017; Quey *et al.*, 2018).

3. Preliminary results and discussion

3.1 Hysteresis of Sm-Co nanostructure and its orientation dependence

Following Katter *et al.* (1996), a parameterized nanostructure for Sm-Co is used. The structure parameters of interest are the Sm_2Co_{17} cell size L, thickness of the stripe-shaped $SmCo_5$ phase w_s, the distance between Z-platelets d, thickness of the Z-platelets w_z and orientation angle α between the field **H** and the easy axis **u**, as shown in Figure 4(a). In this work, we take $L = 150\,\text{nm}$, $d = 50\,\text{nm}$, $w_s = w_Z = 8\,\text{nm}$, while α varies between 0 and $\pi/2$. The nanostructure is generated in a $512 \times 512 \times 4\ \text{nm}^3$ finite difference domain. Periodic BC is applied on the two boundaries perpendicular to the z direction, while Neumann BC is applied on other boundaries. A grain boundary layer with the thickness of 2 nm, where magnetocrystalline isotropy is assumed (i.e. K_{u1}), is also introduced to emulate the effects of the grain boundary in reducing the nucleation field to the system (Yi *et al.*, 2016). To recapture the domain wall behaviors in the micromagnetic simulations without artificial effects related to mesh, the FD cell size is chosen as 0.8 nm, which is smaller than l_{dw}. Micromagnetic parameters of each phase are presented in Table 1.

Figure 4(b) presents a half-cycle hysteresis of a nanostructure with $\alpha = \pi/6$ examined over a single demagnetizing process [H from positive to negative with direction denoted in Figure 4(a)]. The magnetization reversal of the nanostructure consists of two steps: the reversed domain is first generated (nucleated) when the magnetic field reaches a certain threshold, denoted as the nucleation contribution H_c. Then, the nucleated reversed domain starts to grow alongside the reversely increasing magnetic field, demonstrated in the form of domain wall migration. When the migrated domain wall front encounters the intersections between different phases where the domain wall energy differences exist, magnetic energy is consumed to compensate such differences and the domain wall front stops migration, i.e. domain wall pinning occurs. The pinning events are reflected on the hysteresis curve as multiple stages where the magnetization is barely changed, as shown in the Figure 4(b).

Therefore, the extra magnetic field (denoted as pinning contribution H_p) is required for the magnetization reversal.

We further present that the nucleation and pinning events on the nanostructure vary with the orientation angle, even though the parameters of constituent phases do not change. As shown in Figure 4(c), the half-cycle hysteresis curves present varying staging patterns w.r.t. α, resulting in H_{sw} as a function of α as shown in the inset of Figure 4(c). We then take this $H_{sw}(\alpha)$ and feed in the vector hysteron in equation (11) and present its longitudinal magnetization for comparison. We can tell that the hysteron can nicely emulate the magnetization reversal for the coherent case ($\alpha = 0$). For increasing α to $\pi/2$, the hysteron presents an increased deviation in demagnetization compared to the micromagnetic simulation. When $H < H_{sw}$, the hysteron shows less longitudinal demagnetization than the micromagnetic one, implying the relatively slower rotation of the surrogate magnetization vector; when $H > H_{sw}$, the hysteron shows higher longitudinal demagnetization than the micromagnetic one, implying the relatively faster rotation of the surrogate magnetization vector. This difference in the demagnetization process between the hysteron and the micromagnetics eventually leads to the deviation of the magnetic coercivity for $0 < \alpha < \pi/2$. For $\alpha = \pi/2$, both result in zero coercivity, even though the difference in demagnetization process still exists.

3.2 Hysteresis of Sm-Co polycrystal

We apply the surrogate hysterons with micromagnetics-informed $H_{sw}(\alpha)$ in a 10-grain polycrystal structure with the size $100 \times 100 \times 100\ \mu m^3$. It is sufficiently large so that every point inside the polycrystal structure can be conceptually regarded as the homogenized point of the local nanostructure. Figure 5(a) presents the hysteresis loop of the structure with

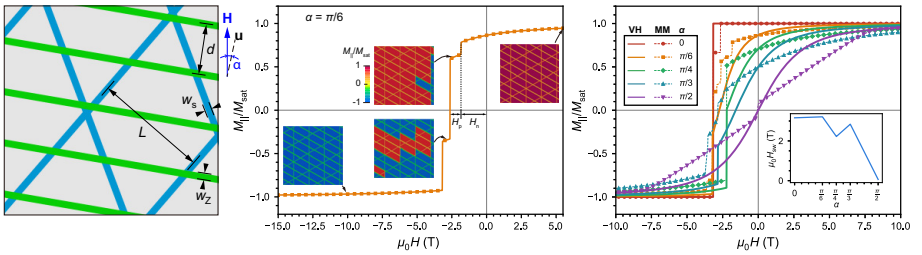

(a) (b) (c)

Source: Authors' own work

Figure 4.
(a) Parameterized nanostructure of Sm-Co magnets. The positive direction of the magnetic field is also denoted; (b) The micromagnetic simulated half-cycle hysteresis of the single demagnetizing process of Sm-Co nanostructure with corresponding domain configuration denoted; (c) Average half-cycle hysteresis of five demagnetizing processes by micromagnetic simulation (MM) for each orientation angle (α), which is compared with parameterized vector hysteron (VH). Inset: orientation dependence of the switching field H_{sw}

Parameters	Unit	Sm_2Co_{17}	$SmCo_5$	Z-platelets[a]
A_{ex}	pJ m^{-1}	19.6	8.6	0.7
K_{u1}	MJ m^{-3}	3.9	18.3	1.4
M_{sat}	kA m^{-1}	987.7	810.8	310.4
l_{dw}	nm	7.0	2.2	2.2
σ_{dw}	mJ m^{-2}	35.0	50.2	4.0

Notes: [a]Rescaled A_{ex} and K_{u1} according to equation (4) by taking the σ_{dw} from literature and the l_{dw} assumed to be coherent with one in $SmCo_5$ phase
Source: Table courtesy of Katter *et al.* (1996)

Table 1.
Micromagnetic parameters for the phases appearing in this work

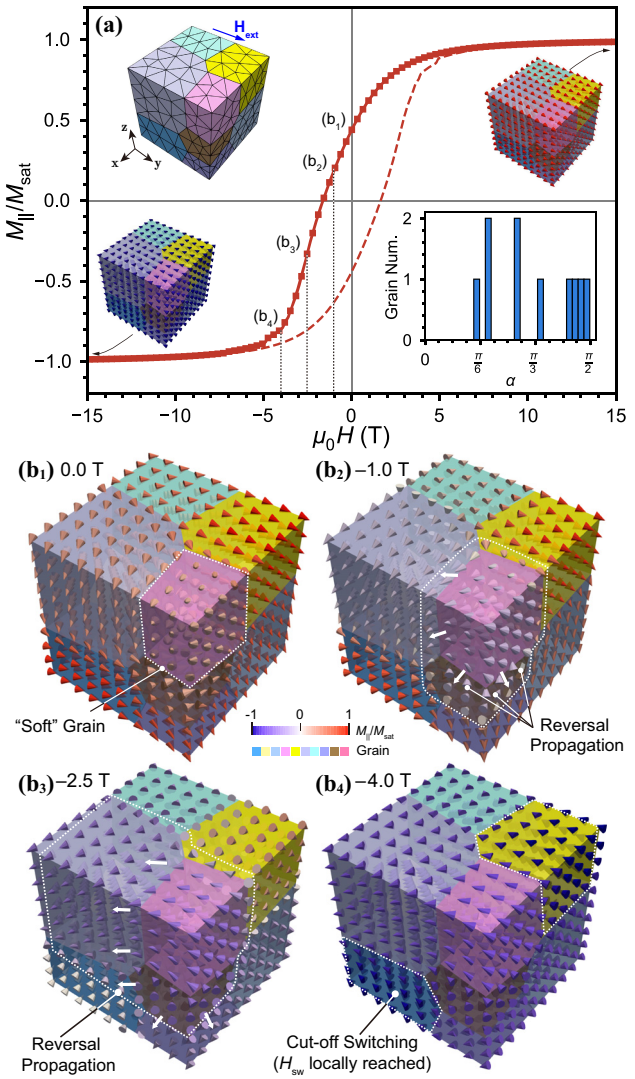

Source: Authors' own work

Figure 5.
(a) The simulated hysteresis loop of the polycrystal structure. Insets: the FE mesh and the orientation histogram of the structure. Local magnetization reversal of sampled points (visualized as rotating cones) is also visualized under different applied field: (b_1) 0.0 T; (b_2) −1.0 T; (b_3) −2.5 T; (b_4) −4.0 T

its mesh and orientation histogram shown in the insets. The magnetic coercivity of the polycrystal reads as 1.65 T, which is smaller than the one of 3.17 T from micromagnetic simulation on the coherent nanostructure (**H**||**u**). This is because more than half of the grains inside the examined polycrystal possess orientation angles that are beyond $\pi/4$, which significantly affect the overall hysteresis of the structure.

To deliver insight into how those grains with relatively larger α affect the demagnetization of the structure, we sample $10 \times 10 \times 10$ points and visualize their on-site hysterons as oriented cones. With the applied magnetic field reduced to zero, we can tell that

the local hysterons inside certain grains [denoted in Figure 5(b_1)] point to the direction almost $\pi/2$ w.r.t. the magnetic field direction, which is also the easy axis of the grain. This grain is regarded as the "soft" grain as the local coercivity inside is nearly zero. The surrounding hysterons receive the influence of the grain and deviate slightly from their stable directions. It is worth noting that the hysterons inside the grain with $\pi/4 < \alpha < \pi/2$ would be affected relatively easier, presenting a trend of reversal propagation toward those directions. When the field starts to reversely increase ($H < 0$), the hysterons inside the "soft" grain already present the reversed magnetization and continue propagating the effect to the surrounded grains with relatively large α, as shown from Figure 5(b_2) to Figure 5(b_3). Meanwhile, the hysterons inside grains with $0 \leq \alpha < \pi/4$ ("hard" grains) receive less effects from already reversed ones, until the local field is large enough to suddenly reverse all of them, as denoted in Figure 5(b_4). This is due to the cut-off switching of those hysterons as demonstrated in Figure 3, where the local field reaches the H_{sw}.

4. Conclusions

We present in this work a novel multiscale simulation scheme for permanent magnets recapitulating its structural and physical characteristics from the nanoscale to the mesoscale. We perform the micromagnetic simulations on the parameterized Sm-Co nanostructures and investigate the mechanisms that are tightly related to the local magnetic coercivity, including the nucleation of the reversed domain, domain wall migration and pinning and unveil the orientation dependence of the demagnetization processes via half-cycle hysteresis curves. This information is then carried by micromagnetics-informed surrogate hysterons in the magnetostatic homogenization of a 10-grain polycrystalline structure with assigned orientations. The simulation results of the polycrystal demonstrate that the grains with largest α ("soft" grains) influence the overall demagnetization process significantly by their early reversing and further propagate such effect to the grains with $\pi/4 < \alpha < \pi/2$ via affecting the local field. This is believed to result in a magnetic coercivity of 1.65 T, which is smaller than the one of 3.17 T examined from coherent nanostructures.

The presented work also showcases the demand of integrating data-driven methods, as the parameters of the surrogate hysteron intrinsically depend on the nanostructure and its orientation. In other words, effects of the nanostructural parameters (here L, d, w_s and w_Z) on the behavior of surrogate hysterons and the sensitivity analysis should be addressed in the upcoming works. More hysteron parameters that further help the surrogate hysteron to emulate the micromagnetic-simulated magnetization reversal, e.g. an orientation-dependent offset that adjusts the demagnetization (or rotation) of the hysteron, should be also discussed and examined.

References

Brown, W.F. Jr, (1963), "Thermal fluctuations of a single-domain particle", *Physical Review*, Vol. 130 No. 5, p. 1677.

Coey, J.M. (2010), *Magnetism and Magnetic Materials*, Cambridge University Press, Cambridge.

Donahue, M.J. and Porter, D.G. (2004), "Exchange energy formulations for 3D micromagnetics", *Physica B: Condensed Matter*, Vol. 343 Nos 1/4, pp. 177-183.

Duerrschnabel, M., Yi, M., Uestuener, K., Liesegang, M., Katter, M., Kleebe, H.-J., Xu, B., Gutfleisch, O. and Molina-Luna, L. (2017), "Atomic structure and domain wall pinning in samarium-cobalt-based permanent magnets", *Nature Communications*, Vol. 8 No. 1, p. 54.

Exl, L., Bance, S., Reichel, F., Schrefl, T., Peter Stimming, H. and Mauser, N.J. (2014), "Labonte's method revisited: an effective steepest descent method for micromagnetic energy minimization", *Journal of Applied Physics*, Vol. 115 No. 17, p. 17D118.

Fangohr, H., Bordignon, G., Franchin, M., Knittel, A., de Groot, P.A. and Fischbacher, T. (2009), "A new approach to (quasi) periodic boundary conditions in micromagnetics: the macrogeometry", *Journal of Applied Physics*, Vol. 105 No. 7.

Gilbert, T.L. (1955), "A Lagrangian formulation of the gyromagnetic equation of the magnetization field", *Phys. Rev*, Vol. 100, p. 1243.

Giron, S., Polin, E., Adabifiroozjaei, Y., Yang, D., Ohmer, R.U., Üstüner, M., Katter, I.A., Radulov, K.P., Skokov, B.-X., Xu, L., Molina-Luna, B. and Gutfleisch, O. (2022), "Investigation of two-step demagnetisation behavior of samarium-cobalt based sintered permanent magnets with high remanence", (preparing).

Goldfarb, D., Wen, Z. and Yin, W. (2009), "A curvilinear search method for p-harmonic flows on spheres", *SIAM Journal on Imaging Sciences*, Vol. 2 No. 1, pp. 84-109.

Gong, Q. (2022), "Multiscale calculations of intrinsic and extrinsic properties of permanent magnets", Ph.D. dissertation, Technische Universität Darmstadt, Darmstadt, available at: http://tuprints.ulb.tu-darmstadt.de/22038/

Gutfleisch, O. (2009), "High-temperature samarium cobalt permanent magnets", *Nanoscale Magnetic Materials and Applications*, pp. 337-372.

Jiles, D.C and Atherton, D.L. (1984), "Theory of ferromagnetic hysteresis (invited)", *Journal of Applied Physics*, Vol. 55 No. 6, pp. 2115-2120.

Katter, M., Weber, J., Assmus, W., Schrey, P. and Rodewald, W. (1996), "A new model for the coercivity mechanism of Sm/sub 2/(Co, Fe, Cu, Zr)/sub 17/magnets", *IEEE Transactions on Magnetics*, Vol. 32 No. 5, pp. 4815-4817.

Kronmüller, H. (2003), *Micromagnetism and the Microstructure of Ferromagnetic Solids*, Cambridge University Press, Cambridge.

Leliaert, J., Dvornik, M., Mulkers, J., De Clercq, J., Milošević, M. and Van Waeyenberge, B. (2018), "Fast micromagnetic simulations on GPU-recent advances made with", *Journal of Physics D: Applied Physics*, Vol. 51 No. 12, p. 123002.

McMichael, R.D., Donahue, M.J., Porter, D.G. and Eicke, J. (1999), "Comparison of magnetostatic field calculation methods on two-dimensional square grids as applied to a micromagnetic standard problem", *Journal of Applied Physics*, Vol. 85 No. 8, pp. 5816-5818.

Permann, C.J., Gaston, D.R., Andrš, D., Carlsen, R.W., Kong, F., Lindsay, A.D., Miller, J.M., Peterson, J.W., Slaughter, A.E., Stogner, R.H. and Martineau, R.C. (2020), "MOOSE: enabling massively parallel multiphysics simulation", *SoftwareX*, Vol. 11, p. 100430.

Petrila, I. and Stancu, A. (2011), "Analytical vector generalization of the classical stoner-Wohlfarth hysteron", *Journal of Physics: Condensed Matter*, Vol. 23 No. 7, p. 76002.

Preisach, F. (1935), "Über die magnetische nachwirkung", *Zeitschrift für Physik*, Vol. 94 Nos 5/6, pp. 277-302.

Quey, R. and Renversade, L. (2017), "Optimal polyhedral description of 3D polycrystals: method and application to statistical and synchrotron X-ray diffraction data", *Computer Methods in Applied Mechanics and Engineering*, Vol. 330, pp. 308-333.

Quey, R., Villani, C. and Maurice, A. (2018), "Nearly uniform sampling of crystal orientations", *Journal of Applied Crystallography*, Vol. 51 No. 4, pp. 1162-1173.

Quey, R., Dawson, P. and Barbe, F. (2011), "Large-scale 3D random polycrystals for the finite element method: generation, meshing and remeshing", *Computer Methods in Applied Mechanics and Engineering*, Vol. 200 Nos 17/20, pp. 1729-1745.

Song, X., Liu, Y., Xiao, A., Yuan, T. and Ma, T. (2020), "Cell-boundary-structure controlled magnetic-domain-wall-pinning in 2:17-type Sm-Co-Fe-Cu-Zr permanent magnets", *Materials Characterization*, Vol. 169, p. 110575.

Sun, J.Z. (2000), "Spin-current interaction with a monodomain magnetic body: a model study", *Physical Review B*, Vol. 62 No. 1, pp. 570-578.

Takács, J. (2001), "A phenomenological mathematical model of hysteresis", *COMPEL – The International Journal for Computation and Mathematics in Electrical and Electronic Engineering*, Vol. 20 No. 4, pp. 1002-1015.

Tonks, M.R., Gaston, D., Millett, P.C., Andrs, D. and Talbot, P. (2012), "An object-oriented finite element framework for multiphysics phase field simulations", *Computational Materials Science*, Vol. 51 No. 1, pp. 20-29.

Vansteenkiste, A., Leliaert, M., Dvornik, M., Helsen, F., Garcia-Sanchez, B. and Van Waeyenberge, J. (2014), "The design and verification of mumax3", *AIP Advances*, Vol. 4 No. 10.

Wang, C. and Zhu, M.-G. (2021), "Overview of composition and technique process study on 2:17-type Sm–Co high-temperature permanent magnet", *Rare Metals*, Vol. 40 No. 4, pp. 790-798.

Yi, M., Gutfleisch, B.X. and Xu, O. (2016), "Micromagnetic simulations on the grain shape effect in Nd-Fe-B magnets", *Journal of Applied Physics*, Vol. 120 No. 3.

Zhou, X., Liu, W., Jia, X., Song, A., Xiao, T., Yuan, F., Wang, J., Fan, T. and Ma, Y. (2021), "Revisiting the pinning sites in 2:17-type Sm-Co-Fe-Cu-Zr permanent magnets", *Journal of Rare Earths*, Vol. 39 No. 12, pp. 1560-1566.

Zirka, S.E., Moroz, R.G., Harrison, K. and Chwastek, Y.I. (2012), "On physical aspects of the Jiles-Atherton hysteresis models", *Journal of Applied Physics*, Vol. 112 No. 4, p. 43916.

Corresponding authors
Yangyiwei Yang can be contacted at: Yangyiwei.yang@mfm.tu-darmstadt.de and Bai-Xiang Xu can be contacted at: xu@mfm.tu-darmstadt.de